Synthesis, characterization and stability of crosslinked chitosan-maltodextrin pH-sensitive nanogels

Karla Gricelda Fernández-Solís, Estefanía Domínguez-Fonseca, Brianda María González Martínez, Alberto Gutiérrez Becerra, Edgar Figueroa-Ochoa, Eduardo Mendizábal, Guillermo Toriz, Pascal Loyer, Julien Rosselgong, Lourdes Monica Bravo-Anaya

Synthesis, Characterization and Stability of Crosslinked Chitosan-Maltodextrin pH-Sensitive Nanogels

Karla Gricelda Fernández-Solís[a,b], Estefanía Domínguez-Fonseca[b,c], Brianda María González Martínez[c], Alberto Gutiérrez Becerra[c], Edgar Figueroa Ochoa[a], Eduardo Mendizábal[a], Guillermo Toriz[d], Pascal Loyer[e], Julien Rosselgong[b], Lourdes Mónica Bravo-Anaya[b*]

[a] Universidad de Guadalajara, Departamento de Química. Blvd. M. García Barragán #1451, C.P. 44430, Guadalajara, Jalisco, México.

[b] Université de Rennes, CNRS, ISCR – UMR 6226, F-35000 Rennes, France.

[c] CUTonalá, Departamento de Ciencias Básicas y Aplicadas, Universidad de Guadalajara, Nuevo Periférico # 555, C.P.45425, Ejido San José Tatepozco, Jalisco, México.

[d] Departamento de Madera, Celulosa y Papel, Universidad de Guadalajara, Camino R. Padilla Sánchez, 2100, Nextipac. 45200 Zapopan, Jalisco, México.

[e] Université de Rennes, Inserm, INRAE, Institut NUMECAN, UMR-A 1341, UMR-S 1317, Plateforme SynNanoVect, Rennes.

Corresponding authors: [*]lourdes-monica.anaya@univ-rennes.fr, Tel: +33-656-886-206.

Abstract

Polysaccharide-based nanogels offer a wide range of chemical compositions and are of great interest due to their biodegradability, biocompatibility, non-toxicity, and their ability to display pH, temperature, or enzymatic response. In this work, we synthesized monodisperse and tunable pH-sensitive nanogels by crosslinking, through reductive amination, chitosan and partially oxidized maltodextrins, by keeping the concentration of chitosan around the overlap concentration, *i.e.* in the dilute and semi-dilute regime. The chitosan/maltodextrin nanogels presented sizes ranging from 63 ± 9 to 279 ± 16 nm, showed quasi-spherical and cauliflower-like morphology, reached a ζ -potential of +36 ± 2 mV and maintained a colloidal stability for up to 7 weeks. It was found that the size and surface charge of nanogels depended both on the oxidation degree of maltodextrins and chitosan concentration, as well as on its degree of acetylation and protonation, the latter tuned by pH. The pH-responsiveness of the nanogels was evidenced by an increased size, owed to swelling, and

ζ-potential when pH was lowered. Finally, maltodextrin-chitosan biocompatible nanogels were assessed by cell viability assay performed using the HEK293T cell line.

Keywords: Nanogels; Chitosan; Maltodextrins; Reductive Amination; pH-sensitive; Overlap concentration

1. Introduction

Hydrogels are polymer networks bearing hydrophilic functional groups that make them capable of holding water within their structure without dissolving in water [1,2]. These polymeric materials are classified as macro, micro and nanogels. Nanogels are hydrogel particles whose dimensions are in the nanoscale, although this size definition might vary according to different authors. Some researchers define nanogels as polymer networks having sizes with less than a micrometer [3,4], others with up to 200 nm [5-7] and others with less than 100 nm [8-10]. In any case, the reduced size of the nanogels is attractive for biomedical applications such as cancer treatments, local anesthetic drug delivery, gene therapy, tissue engineering, and management of diabetes through sustained release of insulin, among others [5,8,11-13].

Nanogels can be synthesized or assembled via chemical or physical methods. Physically crosslinked nanogels are self-assembled through physical interactions between hydrophilic and hydrophobic polymer moieties or by electrostatic interactions between polyanions and polycations [14]. On the other hand, chemically crosslinked nanogels can form polymeric networks by polymerization or crosslinking of polymeric precursors. Polymerization can be carried out by gamma and electron beam polymerization, chain growth, addition or condensation reactions [15]. Crosslinking of polymeric precursors may proceed by click chemistry, Schiff-base reaction, thiol-disulfide exchange, and boronic acid-diol complexation [16].

Nanogels can also be classified according to their polymeric components, *i.e.,* synthetic or natural. Synthetic nanogels can be produced with different chemical and physical properties [17]; however, their biological compatibility for medical applications needs to be improved. Natural nanogels present numerous advantages for applications in the biomedical field, such as biocompatibility, biodegradability and reduced toxicity. Even more, natural polymers originate from abundant natural resources, making them inexpensive and readily available [14,18-20]. Both proteins and polysaccharides (*i.e.,* chitosan, heparin, hyaluronic acid,

chondroitin sulphate, cellulose, dextran, pullulan, and alginate, among others) can be used for this purpose, however polysaccharides are more commonly utilized [21-25].

Chitosan (CS) and maltodextrins (MD) are safe, biocompatible and easily accessible materials. CS is a cationic polymer bearing primary amino groups, responding to pH changes [26], while MDs are starch-derived branched polysaccharides obtained by hydrolysis of starch [27] that have been routinely used as excipients in the pharmaceutical industry [28,29]. Starch-based nanogels for drug delivery, especially for cancer treatment, have been obtained by radiation and chemical crosslinking by amide bonds with natural or synthetic polymers (*i.e.* CS, polyethylene glycol, and hyaluronic acid) [30,31]. The rheological and physicochemical behavior (elastic modulus, swelling, gelation and phase behavior) of MD-based hydrogels have also been reported [32-36] along with biomedical applications such as wound dressing [37] and enzyme delivery [38]. On the other hand, CS nanogels have been proposed for biomedical applications, such as drug delivery systems in oncology. Some of the drugs for cancer treatments transported by CS-based nanogels include methotrexate [39-41], doxorubicin hydrochloride [42,43], fluorouracil [26,44] and pravastatine [45], among others.

Chitosan and starch derivatives have been used to prepare hydrogels, and the kinetics of gelation as well as rheological and swelling behaviors have been reported [45]. However, removal of solvent traces at the end of the preparation process [46] and toxicity of their components remain a challenge in the synthesis of nanogels [47]. Interestingly, polysaccharide-based hydrogels synthesized using chitosan and previously oxidized non-ionic polysaccharides (galactomannan, maltodextrins, methylcellulose) through reductive amination were proposed by Rinaudo [35], leading to the formation of covalent bonds between chitosan and aldehydic substrates, which are stable over the whole range of pH [48]. Reductive amination has been widely used in the synthesis of chitosan-based hydrogels and nanogels with poly(ethylene glycol)dialdehyde for oral protein drug delivery [49], chitosan-gelatin hybrid hydrogels for 3D printable *in vitro* models [50], and N-(furfural) chitosan hydrogels for the development of biological and biomedical applications [51], among others. With these bases, the aim of this work is to take advantage of the molecular parameters of chitosan and polymeric concentration regimes, to synthesize monodisperse, positively charged, stable and pH-sensitive CS/MD nanogels.

Thus, the objective of this work was to synthesize biocompatible-pH-sensitive nanogels by crosslinking CS and oxidized maltodextrins via an adjusted reductive amination reaction. We proposed to maintain the concentration of chitosan below the overlap concentration, *i.e.* in the dilute and semi-dilute regime, in order to obtain reproducible and tunable monodisperse pH-sensitive nanogels. The physicochemical characteristics of CS such as molecular weight (MW), degree of acetylation (DA), and degree of protonation, as well as the degree of oxidation of MD were related to the properties of the resulting nanogels, *i.e.,* size, surface charge, morphology and pH-responsiveness. The design and synthesis of CS-based nanogels is of great relevance for biomedical and pharmaceutical applications.

2. Materials and methods

2.1. Materials

Five CS samples were used to study the effect of MW and DA on the properties of MD/CS nanogels. Three CS samples (provided by Primex, Iceland, ChitoClear®) were from Northern cold-water shrimp (*Pandalus borealis*) had the following characteristics: #1 (MW= 540 000 g/mol, DA= 0.30); #6 (Mw= 160 000 g/mol, DA=0.05); and #8 (Mw=120 000 g/mol, DA=0.47). Two CS samples were purchased from Sigma Aldrich: MMW (Mw= 86 750 g/mol, DA= 0.22, Ref: 44,887-7) and HMW (Mw= 417 600 g/ mol, DA= 0.16, Ref: 41,941-9). The characterization of CS samples from Primex was previously reported by Bravo-Anaya et al [52]. Maltodextrin (purchased from Sigma Aldrich, DE = 16.5-19.5, Ref. 41, 969-9) was analyzed by SEC to estimate its molecular weight. Sodium periodate, ethylene glycol, sodium cyanoborohydride ($NaBH_3CN$), *n*-butylamine, sodium acetate (CH_3COONa), acetic acid glacial (purity ≥99%); hydrochloric acid (37%) and NaOH in pellets with impurities 0.001% were acquired from Sigma Aldrich Company and used as received. A regenerated cellulose dialysis membrane with a molecular weight cutoff (MWCO) of 3.5 kDa was used for the purification of nanogels.

2.2. Preparation of chitosan solutions

In order to obtain fully protonated chitosan solutions, CS (20 mg) was dissolved with the stoichiometric amount of HCl 0.1 N on the basis of the $-NH_2$ content in each CS sample. Hence, depending on the DA of the different CS samples, the obtained stock solutions concentrations were the following: 3.22 mg/mL for CS #1, 4.29 mg/mL for CS #6, 7.65 mg/mL for CS #8, 5.47 mg/mL for MMW and 5.00 mg/mL for HMW. To guarantee the

complete dissolution of CS, the solutions were placed under constant stirring overnight at room temperature. Finally, the vials were sealed with parafilm® and kept under refrigeration at 5 °C to avoid degradation. CS samples used for the synthesis of nanogels were prepared by dilution of the stock solutions to a concentration of 1 mg/mL using sodium acetate buffer (0.1 M). Finally, CS dilutions were adjusted to pH at 3.5 or 5.5. Potentiometric titrations were used to determine the equivalent points and pK_a value of the different chitosan samples. Small volumes of 0.3 mL of NaOH solution at 0.1 M were added progressively to the 100% protonated chitosan solution (0.5 mg/mL, V= 20 mL) while the pH obtained was recorded using a pH meter (Orion Star A212 from Thermo Scientific). The protonation degree of chitosan, defined as DP= C_{NH3^+-R}/C (where C_{NH3^+-R} = concentration of protonated amine groups and C is the total concentration of CS in the solution) as a function of pH was calculated by using the following equation:

$$pK_a = pH - \log((1 - DP)/DP) \quad (1)$$

2.3. Oxidation of maltodextrin

Partial oxidation of MD samples was carried out through the oxidative rupture of glycol units by $NaIO_4$ [53] (Scheme 1a). Solutions of MD (40 mg/mL) and periodate were prepared separately in water and maintained in dark conditions to avoid sodium periodate degradation (for example, for a 30 % oxidation of maltodextrin, 2 g MD dissolved in 50 mL of water, and 0.78 g of $NaIO_4$ in 100 mL water) (Table SI-1 summarizes the experimental conditions for all MD oxidation reactions). $NaIO_4$ solution was added to MD solution, and then stirred for 24 h at room temperature in dark conditions. Ethylene glycol (1.3 mL) was added to quench the oxidation while stirring for 30 minutes. Purification was performed by dialysis (cellulose membranes, MWCO= 3.5 kDa), and stopped after two days when the conductivity was equal to deionized water. Dialysis was monitored with conductivity measurements and stopped after two days when values corresponded to those of deionized water. The reaction product was then recovered by freeze-drying, leading to the obtention of a white powder. The final products were characterized by ^{1}H NMR and FTIR to determine their structure and purity.

The degree of oxidation of maltodextrin was determined by two methods. In the first method, free aldehyde groups were determined with ^{1}H NMR by quantifying the butylamine alkyl side chains linked to the oxidized-Maltodextrin (ox-MD) backbone by reductive amination with sodium cyanoborohydride of ox-MD (Scheme 2). In brief, 20 mg of ox-MD were

solubilized in 4 mL of sodium acetate buffer (0.1 M), at a pH of 5, and at room temperature under gentle stirring. Depending on the targeted degree of oxidation (10 and 30), butylamine (49 or 147 μL) was slowly added into the ox-MD solution under high stirring. Then, 25 equivalents of $NaBH_3CN$, previously solubilized in sodium acetate buffer (0.1 M), were added to the reaction mixture and stirred at 50 °C for 24 h. This procedure was repeated until completing 100 equivalents of $NaBH_3CN$. The resultant solutions were dialyzed using a cellulose membrane at room temperature against deionized water, with four changes during 24 h, and followed up with conductivity measurements, to remove any remaining $NaCNBH_3$. The product was then recovered by freeze-drying. Samples were characterized by ^1H NMR and IR to quantify the appended alkyl chain.

The second method to quantify the degree of oxidation of ox-MD consisted on titration with hydroxylamine hydrochloride ($NH_2OH \cdot HCl$) [55], which upon sample dissolution produces HCl that can be quantified with NaOH and related to aldehyde content in the oxidized maltodextrin. This method represents a rapid and less expensive way to quantify the degree of oxidation of maltodextrins, compared to the first one. This method is defined as the number of oxidized units per 100 elemental units [56], and has been previously used for oxidized polysaccharides such as xanthan gum. The endpoint of the titration can be observed through the color change from red to yellow, using methyl orange as an indicator. The pH change during titration was recorded. Finally, the first derivative was calculated, and the oxidation degree of the maltodextrins was obtained [55].

The degree of oxidation of ox-MD samples was calculated using the Equation (2) [56]:

$$Oxidation\ degree\ (\%) = \frac{V_{NaOH} x C_{NaOH}}{n_{C=O} x\ m/Mw}\ X\ 100 \qquad (2)$$

where V_{NaOH} is the volume of NaOH (0.1 M) consumed at the equivalence point, C_{NaOH} corresponds to the concentration of NaOH solution, $n_{C=O}$ is the possible number of aldehyde groups in the MD sample, m is the dry weight of ox-MD (15 mg) and Mw is 162 g/mol (the molecular weight of anhydrous MD repeating unit).

Infrared Spectroscopy (FTIR). Infrared measurements were performed on an FTIR-Alpha II Bruker spectrometer with an ATR at room temperature. A small amount of each freeze-dried sample without any previous preparation was used to perform each measurement.

^{1}H NMR Spectroscopy. Samples were analyzed using a Jeol ECA 600 spectrometer at 25 °C, using the pulse accumulation of 128 scans and LB parameter of 400 MHz. D_2O was used as a solvent for dissolving each sample at 7 mg/mL. Unmodified and ox-MD samples were characterized with this technique, and their spectra were compared and analyzed with Topspin 4.2.0 software.

Size Exclusion Chromatography (SEC). The weight-average molecular weights of maltodextrin samples were determined through SEC measurements using a Malvern VISCOTEK instrument. Maltodextrin was dissolved in $NaNO_3$ 0.1 M at a concentration of around 1 mg/mL and filtered with a membrane (0.22 μm) before being injected into the Malvern A6000M, Aq GPC/SEC column at a temperature of 25 ◦C. The selected flow rate was 1 mL/min at a temperature of 25°C. The injected volume for each measurement was 100 μL. A light scattering detector (LALS-RALS 270 Dual Detector) was associated with a differential refractometer VE3580 VISCOTEK. The *dn/dc* was equal to 0.145 mL/g.

OriginPro software was used for FTIR and SEC data processing, analysis and graphics elaboration.

2.4. Reductive amination reaction for nanogel synthesis

The crosslinking reaction between CS and ox-MD was performed through a reductive amination reaction (Scheme 1b and 1c). This reaction involves the creation of covalent bonds between the amine of CS and the aldehyde of the ox-MD, using $NaCNBH_3$ as a reducing agent [57]. Nanogels were prepared using stoichiometric ratios of amines and aldehydes. Reductive amination was performed using a dilution of the CS stock solution at 1 mg/mL in a sodium acetate buffer (0.1 M) solution, as CS mother solution. From this solution, the desired CS concentrations, calculated depending on the overlap concentration (C*) of the CS sample, were prepared in the dilute regime with the same buffer solution [58,59]. Sodium acetate buffer was used at two pH for these reactions: 3.5 and 5.5. Then, the necessary amount of ox-MD was weighed, and 2 mL of diluted CS solution in sodium acetate buffer 0.1 M was added (as an example: 3 mg of 10 % ox-MD for 2 mL of CS #1 at a concentration of 0.3 mg/mL and a pH of 3.5, *i.e.* 100 % protonated CS in the solution) (The calculations for the determination of the amount of ox-MD are explained in detail in the supplementary information). The mixture of polysaccharides was gently stirred until complete dissolution. Twenty-five equivalents of $NaCNBH_3$ were added to each reaction vial every 24 hours until 100 equivalents were completed, corresponding to the available NH_2 groups in the CS

solution added for each reaction. Finally, MD/CS nanogels suspensions were dialyzed at room temperature against deionized water, changing four times for 24 h and followed up with conductivity measurements until remotion of unreacted $NaCNBH_3$.

2.5. Physicochemical characterization of nanogels

Size measurements through Dynamic Light Scattering (DLS). DLS measurements were performed using either a kinetic nanoparticle size analyzer VASCO KIN™ (Cordouan Technologies, Pessac, France) with a high stability solid-state laser emitting at 638 nm at room temperature and an angle of 170 ° [60], or with a Malvern Zetasizer NanoZS instrument equipped with a standard HeNe laser emitting at 632.8 nm (Malvern, U.K.), at a temperature of 25 °C, and an angle of 90 °. The correlation functions were averaged from three measurements of 3 runs (60 seconds each one). The equilibration time for this measurement was 60 seconds. The hydrodynamic diameter (D_H) was determined using the Stokes−Einstein equation for spherical particles [61]. Measurements for each sample were performed in duplicate. The obtained results for the size and PDI are presented as mean with the +/- calculated standard deviation.

Charge determination. ζ-potential measurements were carried out with a Malvern Zetasizer NanoZS at a temperature of 25 ºC in a Zetasizer Nano cell (DTS1070). 1 mL of the suspension was injected into the Zetasizer Nano cell for each measurement (performed three times for 100 cycles, with a delay between cycles of 60 s). The equilibration time was 60 s, and ζ-potential was calculated with the Smoluchowski expression, using the electrophoretic mobility values of the nanogels [62]. Measurements for each sample were done in duplicate.

Scanning Electron Microscopy (SEM). SEM observations were performed using a JEOL JSM 7100f microscope. One drop of each nanogel suspension was deposited on a silicon wafer and placed in the oven for 15 min to evaporate the solvent, then sputter coated with Au/Pd for 40 seconds with a Leica EM ACE 200 metallizer. Surface topography images were taken using a SEI secondary electron image detector. The particle size distribution was determined one-by-one using the ImageJ software.

Transmission Electron Microscopy (TEM). TEM images were taken using a JEOL 1400 TEM working at 120 kV and equipped with a GATAN Orius 1000 camera. Samples were prepared by direct deposition of a MD/CS nanogels suspension droplet (7 μL) on carbon grids (300 mesh Cu-300LD from Pacific Grid Tech) up to dry at room temperature. The

particle size distribution was determined by measuring them one-by-one using Image-J software from TEM-micrographs.

Atomic Force Microscopy (AFM). AFM measurements were performed at room temperature in air using atomic force microscope (Multimode Nanoscope 8, Bruker, France). Both topographic and phase images of individual particles were obtained in QMN Mode using a standard silicon cantilever (0.3N/m) and at a scan rate of 1Hz. The scan size was 100*100 μm^2. The force was minimized during all the scans. A drop of suspension was deposited at ambient temperature onto freshly cleaved mica. Measurements of diameter and height were determined using the open-source platform Gwyddion.

OriginPro software was used for DLS and ζ-potential data processing, analysis and graphics elaboration, as well as particle size distribution determination for the analysis of microscopy results (SEM and TEM).

2.6. pH response of nanogels

Potentiometric titration, ζ-potential and DLS measurements were used to follow the response to pH of MD/CS nanogels by progressive addition of HCl 0.1 N into MD/CS nanogel suspension at initial pH of around 7. Mettler Toledo pH/conductivity meter SG23 was used to determine the changes in pH. After stabilization of the initial pH, 1 mL of the solution was injected into the Zetasizer Nano cell for ζ-potential measurement and then for a DLS measurement. Nanogels suspensions were collected after each measurement from the cell and reintroduced into the bulk suspension before the addition of the next volume of HCl.

2.6. Cell viability

The *in vitro* studies were performed using the human embryonic kidney HEK293T cells, which are widely used in cell biology because of their rapid growth [63]. HEK293T cell line was cultured in DMEM supplemented with 10% fetal bovine serum (FBS), L-Glutamine, and antibiotics. Every week, the cells were detached using a trypsin solution (0.05%, Gibco) and seeded at a density of 2 x 10^4 cells/cm^2. The culture medium was renewed every 2 days. HEK293T cells were seeded one day prior to the experiment in two 24-well plates at a density of 2 x 10^4 cells/cm^2. Cell viability was assessed by measuring the relative intracellular ATP content using CellTiter-Glo Luminescent Cell viability assay (Promega, Madison, WI, USA – Charbonnières Les Bains, France). After 48 hours of exposure to nanogels, unexposed (control cultures) and exposed cells were incubated with the CellTiter-

Glo reagent for 10 minutes. Lysates were transferred to an opaque multi-well plate and luminescent signals were quantified at 540 nm using the Polarstar Omega microplate reader (BMG Labtech, Champigny sur Marne, France). Cell viabilities in nanogel-exposed cells were expressed as the percentage of the luminescent values obtained in untreated cells, which was arbitrarily set as 100%.

3. Results and discussion

3.1. Maltodextrin oxidation

Maltodextrin molecular weight was firstly determined by SEC measurements. The weight-average molecular weight was 24, 914 g/mol, with a Đ of 1.47 (Fig. SI-1). MDs were oxidized at room temperature with different amounts of periodate in order to vary the degree of oxidation. Oxidized MDs were obtained with a yield of around 32 %. Hydroxyl groups on carbons 2 and 3 of the MD repeat unit were oxidized by sodium periodate, forming two aldehyde groups in each oxidized monomeric unit due to carbon–carbon bond rupture (Scheme 1a). The selected molar ratios [monosaccharide unit]/[periodate] were: 10, 5, 3.3 and 2, corresponding to the targeted degrees of oxidation of 10, 20, 30 and 50 % (at maximum one sugar unit from the maltodextrin can be oxidized over two units). We expected to obtain a greater rotational freedom and new reactive groups for chemical modifications, mainly by reductive-amination reactions, along the maltodextrin backbone [53].

Fig. 1 shows FTIR spectra of the original MD and the resulting ox-MD samples. The sugar ring, common to all samples, is observed in the absorption bands at 3282 and 2927 cm^{-1} corresponding to the stretching vibration of -OH and -CH_2 groups [64]. The C-H bending vibration is confirmed by the absorption bands at 1460 cm^{-1} and 1300 cm^{-1} [65]. The oxidative process of MD can be followed by the appearance of the band at 1723 cm^{-1}, assigned to the stretching of the C=O group [35,64,65]. This band is absent in the original MD, and its relative intensity increases with the degree of oxidation, in good agreement with previous results from Rinaudo for oxidized methylcelluloses [66].

Oxidized polysaccharide samples are expected to display changes in the ^1H NMR spectrum after oxidation, according to their structure. As an example, changes were reported on H1 and H5 signals for (1–4)-β-D-mannuronic acid (M) and (1–4)-α-L-guluronic acid (G) units

of alginate [67], and also the appearance of a signal at around 8.5 ppm, related to protons from aldehydic groups on C-2 or C-3 positions for methylcelluloses [66].

Fig. 2 shows the ^{1}H NMR spectra of the initial MD (Fig. 2a) and ox-MD resulting products with a targeted degree of oxidation of 10 % (Fig. 2b) and 30 % (Fig. 2c). The appearance of signals located between 8 and 9 ppm, attributed to the aldehyde groups present in the oxidized units on the MD, are in good agreement as for methyl cellulose [66]. This signal increased as the degree of oxidation became higher. Furthermore, the appearance of another new signal between 4.8 and 5.3 ppm may indicate the existence of a hydrated aldehyde, where a water molecule was added to the carbonyl group (gem diol), which seems to be the only existing form of the reducing end in water [68]. No aldehyde groups were identified in ^{13}C NMR (data not shown) most probably due to equilibrium in D_2O between the aldehydic form and the hydrated form [35,69]. Ox-MD samples were also analyzed by SEC; right angle light scattering (RALS, 90° light scattering) traces for ox-MD resulting products with targeted oxidation degrees of 10 and 30 % are shown in Fig. SI-1a and Fig. SI-1b. Size exclusion chromatograms show that MD samples preserve their molecular weight distribution after oxidation.

The degree of oxidation of two ox-MD with target oxidation degrees of 10 and 30 % were determined with ^{1}H NMR after a reductive amination reaction between partial ox-MD and butylamine (Scheme 2). Fig. SI-2 and SI-3 show the ^{1}H NMR spectra obtained for the reductive amination products between ox-MD and butylamine, and compared with the original MD and the corresponding oxidation products for targeted oxidation degrees of 10 and 30 %. One can observe the disappearance of the peaks between 8 and 9 ppm and between 4.8 and 5.3 ppm, corresponding to the aldehyde and hydrated aldehyde groups, respectively, present in the ox-MD, as well as the appearance of 3 peaks between 0.9 and 2.0 ppm, which can be attributed to the presence of the protons of the alkyl side chains from butylamine. The quantification of the actual oxidation degrees for the two ox-MD samples was accomplished using the integrals of the peaks corresponding to the protons of the alkyl side chains (either the $-CH_2$ or the $-CH_3$). The oxidation degrees of the ox-MD samples with targeted oxidation degrees of 10 and 30 % were 11 and 48 %, respectively. The molar ratios [monosaccharide units]/[periodate] of the selected ox-MD, corresponding to both degrees of oxidation, are 9.1 and 2.1

Potentiometric titrations using hydroxylamine chloride and methyl orange as indicator, were used to quantify the aldehyde content for all the obtained ox-MD samples. Fig. SI-4a to SI-4d show the pH evolution of the titrated liquid and its first derivative. The degrees of oxidation calculated from Equation (1) for 2 hours reaction (as used by Paiva et al. for xanthan gum) are summarized in Table 1 [55]. The degrees of oxidation obtained from the reductive amination with butylamine by ^{1}H NMR are in good agreement with the values calculated using the hydroxylamine hydrochloride titration method.

3.2. Synthesis of MD/CS nanogels

MD/CS nanogels were synthesized using a reductive amination reaction between CS and ox-MD, as depicted in Scheme 1b. The samples ox-MD with a degree of oxidation of 11 and 48% were selected for the synthesis. A great advantage is that the covalent bonds between CS and ox-MD (*i.e.,* $-NH_2 + R\text{-}HC{=}O \rightarrow -NH\text{-}CH_2\text{-}R$) are stable over the entire pH range [35]. pH at 3.5 and 5.5 were selected for the synthesis of nanogels in sodium acetate buffer (0.1 M). At pH 3.5, all the amino groups in the CS chains are protonated (NH_3^+). On the other hand, the extent of protonation of amino groups at pH 5.5, determined by potentiometric titration, ranged from 41-73% as seen in Table 2 [52].

The synthesis of monodisperse MD/CS nanogels depends on the concentration regime of CS solutions. It is known that below the overlap concentration (C*) polymer chains are separated [69,70]. Moreover, the overlap concentration is related to the viscosity of polymeric samples in solution [57,71], and consequently to the intrinsic viscosities, [η]. From CS [η], previously determined [52], the overlap concentration was found using the relation $C^*[\eta] \approx 1$ [58,70,71]. Six CS concentrations were tested, *i.e.,* C*/5, C*/2, C*, 2C*, 3C* and 5C*. At these conditions, once the crosslinking is carried out, nanoparticles ought to be formed. As an example, Fig. 3 shows the evolution of the intensity distribution as a function of the hydrodynamic diameter for MD/CS nanogels using HMW CS at the six aforementioned concentrations. It can be seen that at CS concentrations lower than C* (0.08 and 0.20 mg/mL), MD/CS nanogels present a bimodal distribution. However, for CS concentrations equivalent to 2C* and 3C* (0.80 and 1.20 mg/mL), monodisperse distributions of 149 ± 4 and 163 ± 2 nm, and PDI of 0.260 and 0.290, respectively, were observed for each sample. Hence, it was determined that CS concentrations in the dilute and semi dilute (unentangled) regime can be used for synthesis of monodisperse MD/CS nanogels, in good agreement with the size range proposed by Yin et al., *i.e.,* from 20 to 250

nm [19]. Akiyama et al. and Neamtu et al. defined as acceptable nanogel dimensions in the wide range of 10−1000 nm, whereas other researchers reported an ideal size of up to 200 nm, in particular for tissue engineering applications [4,12,72,73]. Furthermore, Manivong et al. reported the synthesis of monodisperse CS-based nanogels as drug-delivery platforms nanogels, with sizes ranging from 268 to 382 nm, according to the acidic solution used (*i.e.,* either citric or acetic acid) with an overall surface charge [47]. Finally, it can be said that at higher CS concentration, solution viscosities increase and polydisperse samples were obtained after reductive amination with Ox-MD.

3.3. Effect of the degrees of protonation and acetylation of chitosan and oxidation degree of maltodextrins on the size of MD/CS nanogels

The size of MD/CS nanogels may be controlled both by CS and MD features such as molecular weight, degree of acetylation, concentration, degree of protonation (tuned by pH) and MD degree of oxidation. Table 4 summarizes the D_H and PDI, determined through DLS, for some representative MD/CS nanogels synthesized using different concentrations of CS # 1, CS # 6 and CS # 8, at pH 3.5 and 5.5 and MD oxidation degrees of 11 and 48 %. It was observed that the oxidation degree of MD and the pH of CS solution had an important effect on particle size and surface charge of MD/CS nanogels. Chitosan #6 (Mw= 160 000 g/mol, DA=0.05) was the sample that generated MD/CS nanogels with lower particle sizes (63 ± 9 nm) and a PDI of 0.155 ± 0.050. This CS sample has a molecular weight similar to that of sample #8 (Mw=120 000 g/mol, DA=0.47), but a 10-fold lower degree of acetylation (DA=0.05), hence having a larger content of amino groups allowing for a more compact nanogel (Fig. 4a).

The selected pH for the synthesis of MD/CS nanogels also influenced the particles size. Indeed, for almost all MD/CS nanogels, the D_H is smaller when nanogels are prepared at a pH of 5.5 (Fig. 4b). Reductive amination reactions are pH-dependent and are generally performed at pH ~ 5, typically using a weak acid [74]. Here, the synthesis of MD/CS nanogels at a pH of 5.5 seems to be the most efficient, leading to smaller particle sizes with a high crosslinking degree. Furthermore, MD/CS nanogels synthesized with the ox-MD at 48 % presented smaller sizes than MD/CS nanogels synthesized with the MD sample having low oxidation degree (Fig. 4c). Here, the reductive amination reaction between NH_2 groups from CS will create a denser network of crosslinked CS and ox-MD chains. This behavior is in good agreement with oxidized methylcellulose samples, in which a higher oxidation

degree resulted in a higher degree of crosslinking, forming particles with a lower degree of swelling [66].

3.4. Effect of the degrees of protonation and acetylation of chitosan, concentration and pH during nanogels synthesis on ζ-potential of MD/CS nanogels

ζ–potential is an indicator of the stability of nanoparticles suspensions, such as nanogels [75]. Aggregation of the nanogels in solution will be prevented with a higher electric charge, due to the strong repulsion between particles. Table 5 summarizes the ζ-potential, determined through electrophoretic mobility, of some representative MD/CS nanogels. ζ-potential of MD/CS nanogels was found to be positive for all the samples, due to the cationic contributions of CS. ζ-potential shows a dependence on the degrees of acetylation and protonation (directly related to pH) of CS. At a lower degree of acetylation the ζ-potential was higher owed to be a higher number of amino groups susceptible to protonation in each chitosan chain. CS #6 (DA=0.05) was the sample that generated MD/CS nanogels with higher ζ-potential, *i.e.,* +36 ± 2 mV, followed by CS #1 (DA=0.30) generating MD/CS nanogels with ζ-potential up to +30 ± 1.5 mV.

The surface charge of MD/CS nanogels was also influenced by the pH selected during the synthesis of MD/CS nanogels: the highest ζ-potential were obtained for nanogels synthesized at the lowest pH. As expected, all MD/CS nanogels synthesized with CS solutions at a pH 3.5, at which the polysaccharide presents a 100 % protonation degree, present ζ-potential higher than MD/CS nanogels synthesized with CS solutions at a pH of 5.5. All the comparisons were done with nanogels synthesized with the same ox-MD oxidation degree. The obtained results from ζ-potential are in good agreement with what was expected from the CS charge as a function of pH, as reported in the literature, *i.e.,* a fully protonated CS solution, presents a high ζ-potential, because under these conditions, CS is strongly positively charged [52]. Then, as pH increases, the fraction of [NH_3^+] in CS solution decreases to null charge, thereby decreasing ζ-potential to zero [52].

Also, the ζ-potential of MD/CS nanogels depended on the CS concentration. It is possible to observe that the surface charge of MD/CS nanogels prepared with the three CS samples increased with the increase of CS concentration. Nanogels prepared with CS #6 (DA=0.05) reached a ζ-potential up to +34 ± 1 mV with the highest CS concentration (1 mg/mL), even at the pH (5.5), whereas nanogels prepared with CS #8 (DA=0.47, the lowest from the CS

samples series) reached a ζ-potential up to +22 ± 0.3 mV, with the highest CS concentration (1.4 mg/mL). According to the literature, protonated CS in nanogels, led to the generation of positively charged particles, improving cell membrane infiltration and internalization [76,77]. This feature will be inspected in a further study.

3.5. Morphology of MD/CS nanogels

Particle size and shape of nanogels are important for drug delivery applications and have a great influence on particle distribution in the body [78]. Fig. 5a shows, as an example, a SEM image taken for MD/CS nanogels synthesized using CS #1 (C_{CS}= 1 mg/mL, DA=0.30, pH=5.5) and 48 % ox-MD. The zoom-in presented in Fig. 5b allows the identification of the morphology of dried MD/CS nanogels, which was related to a quasi-spherical shape with a cauliflower-like structure (Fig. 5b). Similar morphologies have been reported for nanogels based on hydroxypropyl cellulose–poly(itaconic acid) [79] and for N,N'-bis(acryloyl)cystamine-based polymers, which also present a peculiar shape and surface rugosity with a cauliflower-like structure [80]. Particle size distribution determined from SEM images analysis (Fig. 5c) showed apparent diameters of 95 ± 21 nm (50 particles), in fair agreement with the D_H determined through DLS measurements, *i.e.* 83 ± 2 nm. Aggregated particles observed in the SEM image may presumably be the reason on the size difference with the obtained value of the hydrodynamic diameter in the solvated state through DLS measurements. Similar morphology, size and size distribution were observed with TEM and AFM for MD/CS nanogels synthesized using CS #1 (C_{CS} = 1 mg/mL, DA = 0.30, pH = 5.5) and 48 % ox-MD (Fig SI-5).

3.6. Stability over time of MD/CS nanogels, pH sensitivity and cell viability

The colloidal stability of MD/CS was monitored through the evolution of the hydrodynamic diameter (D_H) of the particles over time. Fig. 6a and 6b show, as an example, the intensity distribution as a function of D_H measured each week, and the evolution of D_H and PDI as a function of time, respectively, for nanogels prepared with CS HMW (C_{CS}= 1.2 mg/mL, DA=0.16, pH=5.5) and 48 % ox-MD. No aggregation on MD/CS nanogels was observed during 7 weeks. It was also possible to observe that the D_H of MD/CS nanogels remained stable up to 4 weeks after the synthesis. Starting from week #1, the D_H increases from around 163 nm to around 180 nm. This behavior was consistent for different MD/CS nanogels monitored during 7 weeks.

Nanogels can be designed to respond to different stimuli, such as temperature, pH, ionic strength, light, or redox conditions, leading to a controlled release of encapsulated drugs [81,82]. With the presence of amino groups in the CS structure, it is expected that MD/CS nanogels will display a pH response. At low pH, CS amino groups are protonated, leading to the swelling of the nanogel due to its hydrophilicity, electrostatic repulsions between NH_3^+ positively charged groups, as well as the rise of internal osmotic pressure [83]. Then, as the pH increases, deprotonation of CS amino groups reduces the hydrophilicity, leading to a decrease in nanogel size. Fig. 6c shows the evolution of the hydrodynamic diameter and ζ-potential as a function of pH for MD/CS nanogels synthesized with CS HMW (C_{CS} = 1.2 mg/mL, DA = 0.16, pH = 5.5) and 48 % ox-MD. ζ-potential increased progressively to higher positive values (up to + 35 mV) corresponding to a better stability of MD/CS nanogels due to CS protonation. Concomitantly, the pH of the medium decreased from 7.08 to 3.50, mimicking the behavior of nanogels in an acidic medium as they encounter in the cells, where the pH range of endosomal release varies from 7 to 4.5. Then, an increase in MD/CS nanogels D_H was observed at the same time as the pH decreased, while CS amino groups get protonated. A 118% swelling for MD/CS nanogels was determined through DLS measurements when nanogels underwent a pH stimulus, from a pH of 7.08 (D_H = 165 nm) to a pH of 4.2 (D_H = 360 nm). As reported in the literature, this pH-sensitive swelling behavior conferred by CS is suitable for the release of antineoplastic drugs, since nanogels remain collapsed at physiological pH, retaining the drug inside their polymeric network, and then swelling at endosomic pH, leading to its release [26]. The objectives of an ongoing study are the encapsulation of drugs in MD/CS nanogels and the analysis of the release profiles at different pH.

Maltodextrin, chosen to react with chitosan, is a biocompatible polysaccharide, which allows assuming that the obtained nanogels will remain biocompatible. In order to provide a first evaluation of the biocompatibility of the synthesized MD/CS nanogels a cell viability assay was performed. Cell viability was determined by means of the relative ATP content of HEK293T cell in presence of two different nanogels. We observed slight differences in the relative ATP contents in HEK293T cells exposed to nanogels 1 and 2 for 48 hours compared to values obtained in unexposed cells but none of these changes were statistically significant. These data indicated that the nanogels were not cytotoxic toward HEK293T cells in this experimental setting.

4. Conclusion

pH-sensitive nanogels were successfully synthesized by crosslinking, via reductive amination, CS and oxidized MD. Around the overlap concentration of chitosan solutions, *i.e.,* in the dilute and semi-dilute regime, it was possible to obtain monodisperse nanogels. The size and surface charge of nanogels was tuned by modulating the physicochemical characteristics of CS such as DA and degree of protonation CS, as well as the degree of oxidation of maltodextrins. Synthesis at pH 3.5, CS concentrations in the unentangled regime, low DA and high maltodextrin oxidation resulted in smaller nanogels. ζ-potential showed a dependence on the DA of CS and degree of protonation. The highest ζ-potential values were obtained for nanogels synthesized at lowest pH 3.5. The concentration of CS determined the ζ-potential: more concentrated CS solutions resulted in higher ζ-potential. The morphology of the nanogels was quasi-spherical cauliflower-like. Swelling and increased ζ-potential upon decreased pH demonstrate the pH sensitivity of nanogels. Finally, the nanogels were found to be biocompatible using cell viability assays performed with HEK293T cell line.

The experimental results of this study provide information for the design and synthesis of CS-based or polysaccharide-based nanogels for various applications in biomedical and pharmaceutical industries. This study represents the basis of an ongoing study about doxorubicin encapsulation in MD/CS nanogels and the analysis of the release profiles *in vitro* at different pH.

Acknowledgements

The authors of this work acknowledge Loïc Joanny from the ScanMat platform CMEBA for SEM analysis, Agnès Burel from Microscopy Rennes Imaging Center (MRic) of the UMS Biosit (FBI member, ANR-10-INBS-04), University of Rennes for TEM analysis, Véronique Vié from the Institute of Physics of Rennes for AFM measurements and Marielle Blot from the Institute of Chemical Sciences of Rennes for SEC measurements. Karla Gricelda Fernández-Solís acknowledges CONACYT (CVU 1149424), the Laboratory of Rheology and the Laboratory of Modular Projects from the University of Guadalajara and the Institute of Chemical Sciences of Rennes for technical facilities to carry on the research. Lourdes Mónica Bravo-Anaya acknowledges the IEA P_2NanoBio founded by the CNRS as well as Dr. Marguerite Rinaudo for helpful scientific discussions. The authors acknowledge Mrs

H.L. Lauzon from Primex Cy (Iceland) and G. Roberts (England) for the gift of chitosan samples.

References

1. A. Vashist, S. Ahmad, Smart materials for drug delivery, Orient J Chem 29(3) (2013) 861–870. http://doi.org/10.13005/ojc/290303

2. E.M. Ahmed, Hydrogel: preparation, characterization, and applications: a review, J Adv Res 6(2) (2015) 105–121. http://doi.org/10.1016/j.jare.2013.07.006

3. L. Zha, B. Banik, F, Alexis, Stimulus responsive nanogels for drug delivery, Soft Matter 7(13) (2011) 5908–5916. https://doi.org/10.1039/C0SM01307B

4. E. Mauri, G. Perale, F. Rossi, Nanogel functionalization: a versatile approach to meet the challenges of drug and gene delivery, ACS Appl Nano Mater 1(12) (2018) 6525–6541. https://doi.org/10.1021/acsanm.8b01686

5. F. Sabir, M.I. Asad, M. Qindeel, I. Afzal, M.J. Dar, K.U. Shah, F. Din, Polymeric nanogels as versatile nanoplatforms for biomedical applications, J Nanomater 2019 (2019) 1–16. https://doi.org/10.1155/2019/1526186

6. S. Shah, N. Rangaraj, K. Laxmikeshav, S. Sampathi, Nanogels as drug carriers – Introduction, chemical aspects, release mechanisms and potential applications, Int J Pharm 581 (119268) (2020) 1-16. https://doi.org/10.1016/j.ijpharm.2020.119268

7. J. Saloni, A.R. Kumar, S. Saumya, S.S. Lal, S. Mukesh, An overview of nanogel-novel drug delivery system, Asian J Pharm Res Dev 7(2) (2019) 47–55. http://doi.org/10.22270/ajprd.v7i2.482

8. A. V. Kabanov, S. V. Vinogradov, Nanogels as pharmaceutical carriers: Finite networks of infinite capabilities. Angew Chemie - Int Ed, 48(30) (2009) 5418–5429. https://doi.org/10.1002/anie.200900441

9. Y. Sasaki, K. Akiyoshi, Nanogel engineering for new nanobiomaterials: from chaperoning engineering to biomedical applications, Chem Rec 10(6) (2010) 366–376. https://doi.org/10.1002/tcr.201000008

10. K.S. Soni, S.S. Desale, T.K. Bronich, Nanogels: an overview of properties, biomedical applications and obstacles to clinical translation. J Control Release 240 (2016) 109–126. http://doi.org/10.1016/j.jconrel.2015.11.009

11. R.T. Chacko, J. Ventura, J. Zhuang, S. Thayumanavan, Polymer nanogels: a versatile nanoscopic drug delivery platform, Adv Drug Deliv Rev 64(9) (2012) 836–851. http://doi.org/10.1016/j.addr.2012.02.002

12. I. Neamtu, A.G. Rusu, A. Diaconu, L.E. Nita, A.P. Chiriac, Basic concepts and recent advances in nanogels as carriers for medical applications, Drug Deliv 24(1) (2017) 539–557. https://doi.org/10.1080/10717544.2016.1276232

13. E. Sharmin, Medical applications of nanogels. In: A. Vashist, A.K. Kaushik, S. Ahmad, M. Nair, editors, Nanogels for biomedical applications, Royal Society of Chemistry, London, U.K., 2018, pp. 29–52. https://doi.org/10.1039/9781788010481-FP009

14. A.P. Chiriac, A. Ghilan, I. Neamtu, L.E. Nita, A.G. Rusu, V.M. Chiriac, Advancement in the biomedical applications of the (nano)gel structures based on particular polysaccharides. Macromol Biosci 19(9) (2019) 1–20. https://doi.org/10.1002/mabi.201900187

15. M. Suhail, J.M. Rosenholm, M.U. Minhas, S.F. Badshah, A. Naeem, K.U. Khan, M. Fahad, Nanogels as drug-delivery systems: a comprehensive overview, Ther Deliv 10(11) (2019) 697–717. https://doi.org/10.4155/tde-2019-0010

16. X. Zhang, S. Malhotra, M. Molina, R. Haag, Micro- and nanogels with labile crosslinks-from synthesis to biomedical applications, Chem Soc Rev 44(7) (2015) 1948–1973. https://doi.org/10.1039/C4CS00341A

17. E. Mauri, S.M. Giannitelli, M. Trombetta, A. Rainer, Synthesis of Nanogels: Current Trends and Future Outlook, Gels 7(36) (2021) 1-23. https://doi.org/10.3390/gels7020036

18. M.S. Hamid Akash, K. Rehman, S. Chen, Natural and synthetic polymers as drug carriers for delivery of therapeutic proteins, Polym Rev 55(3) (2015) 371–406. https://doi.org/10.1080/15583724.2014.995806

19. Y. Yin, B. Hu, X. Yuan, L. Cai, H. Gao, Q. Yang, Nanogel: A versatile nano-delivery system for biomedical applications, Pharmaceutics 12(3) (2020) 290–315 https://doi.org/10.3390/pharmaceutics12030290

20. J. Yang, S. Han, H. Zheng, H. Dong, J. Liu, Preparation and application of micro/nanoparticles based on natural polysaccharides. Carbohydr Polym 123 (2015) 53–66. https://doi.org/10.1016/j.carbpol.2015.01.029

21. T.A. Debele, S.L. Mekuria, H.C. Tsai, Polysaccharide based nanogels in the drug delivery system: Application as the carrier of pharmaceutical agents, Mater Sci Eng C 68 (2016) 964–981. http://doi.org/10.1016/j.msec.2016.05.121

22. N. Kamaly, B. Yameen, J. Wu, O.C. Farokhzad, Degradable controlled-release polymers and polymeric nanoparticles: mechanisms of controlling drug release, Chem Rev 116(4) (2016) 2602–2663. https://doi.org/10.1021/acs.chemrev.5b00346

23. D. Pamfil, C. Vasile, Nanogels of natural polymers. In: V.K. Thakur, M. Thakur, S. Voicu, editors, Polymer gels, Springer, Singapore, 2018, pp. 71–110. https://doi.org/10.1007/978-981-10-6080-9_4

24. A. Srivastava, T. Yadav, S. Sharma, A. Nayak, A. Kumari, N. Mishra, Polymers in drug delivery, J Biosci Med 4 (2016) 69–84. https://doi.org/10.4236/jbm.2016.41009

25. S. Uthaman, S. Maya, R. Jayakumar, C.S. Cho, I.K. Park, Carbohydrate-based nanogels as drug and gene delivery systems. J Nanosci Nanotechnol 14(1) (2014) 694–704. https://doi.org/10.1166/jnn.2014.8904

26. M. Arteche Pujana, L. Perez-Alvarez, L.C. Cesteros Iturbe, I. Katime, PH-sensitive chitosan-folate nanogels crosslinked with biocompatible dicarboxylic acids, Eur Polym J 61 (2014) 215–225. http://doi.org/10.1016/j.eurpolymj.2014.10.007

27. C. Garnero, C. Aloisio, M. Longhi, Ibuprofen-maltodextrin interaction: study of enantiomeric recognition and complex characterization, Pharmacol Pharm 4(01) (2013) 18–30. https://doi.org/10.4236/pp.2013.41003

28. S. Barthold, M. Hittinger, D. Primavessy, A. Zapp, H. Groß H, M. Schneider, Preparation of maltodextrin nanoparticles and encapsulation of bovine serum albumin – Influence of formulation parameters, Eur J Pharm Biopharm 142 (2019) 405–10. https://doi.org/10.1016/j.ejpb.2019.07.003

29. Q. Jin, S. Maji, S. Agarwal, Novel amphiphilic, biodegradable, biocompatible, cross-linkable copolymers: Synthesis, characterization and drug delivery applications, Polym Chem 3(10) (2012) 2785–2793. https://doi.org/10.1039/c2py20364b

30. P. Saracoglu, M.M. Ozmen, Starch based nanogels: from synthesis to miscellaneous applications, Starch/Staerke 73(9–10) (2021) 1–10.: https://doi.org/10.1002/star.202100011

31. D. Binh, P.T.T. Hong, N.N. Duy, N.T. Duoc, N.N. Dieu, A study on size effect of carboxymethyl starch nanogel crosslinked by electron beam radiation, Radiat Phys Chem 81(7) (2012) 906–912. http://dx.doi.org/10.1016/j.radphyschem.2011.12.016

32. P.A.M. Steeneken, A.J.J. Woortman, Superheated starch: a novel approach towards spreadable particle gels, Food Hydrocoll 23(2) (2009) 394–405. https://doi.org/10.1016/j.foodhyd.2008.01.006

33. F. Masullo, Y. Beldengrün, J. Miras, A.D. Mackie, J. Esquena, J.B. Avalos, Phase behavior of gelatin/maltodextrin aqueous mixtures studied from a combined experimental and theoretical approach, Fluid Phase Equilib 524 (2020) 112675 1-12. https://doi.org/10.1016/j.fluid.2020.112675

34. M.T. Nickerson, R. Farnworth, E. Wagar, S.M. Hodge, D. Rousseau, A.T. Paulson, Some physical and microstructural properties of genipin-crosslinked gelatin-maltodextrin hydrogels, Int J Biol Macromol 38(1) (2006) 40–4. https://doi.org/10.1016/j.ijbiomac.2005.12.017

35. M. Rinaudo, New way to crosslink chitosan in aqueous solution, Eur Polym J 46(7) (2010) 1537–1544. https://doi.org/10.1016/j.eurpolymj.2010.04.012

36. C. Loret, V. Meunier, W.J. Frith, P.J. Fryer, Rheological characterisation of the gelation behaviour of maltodextrin aqueous solutions, Carbohydr Polym 57(2) (2004) 153–163. https://doi.org/10.1016/j.carbpol.2004.03.026

37. H.I. Meléndez-Orti, R. Betancourt-Galindo, B. Puente-Urbina, A. Ledezma, O. Rodríguez-Fernández, Synthesis and characterization of hydrogels based on maltodextrins with antimicrobial properties, Int J Polym Mater Polym Biomater 0(0) (2021) 1–10. https://doi.org/10.1080/00914037.2021.1931209

38. Y. Beldengrün, J. Aragon, S.F. Prazeres, G. Montalvo, J. Miras, J. Esquena, Gelatin/maltodextrin water-in-water (W/W) emulsions for the preparation of cross-linked enzyme-loaded microgels, Langmuir 34(33) (2018) 9731–9743. https://doi.org/10.1021/acs.langmuir.8b01599

39. H. Ashrafi, A. Azadi, Chitosan-based hydrogel nanoparticle amazing behaviors during transmission electron microscopy, Int J Biol Macromol 84 (2016) 31–34. http://dx.doi.org/10.1016/j.ijbiomac.2015.11.089

40. A. Azadi, M. Hamidi, M.R. Rouini, Methotrexate-loaded chitosan nanogels as "Trojan Horses" for drug delivery to brain: Preparation and in vitro/in vivo characterization, Int J Biol Macromol 62 (2013) 523–530. http://doi.org/10.1016/j.ijbiomac.2013.10.004

41. A. Azadi, M.R. Rouini, M. Hamidi, Neuropharmacokinetic evaluation of methotrexate-loaded chitosan nanogels, Int J Biol Macromol 79 (2015) 326–335. http://doi.org/10.1016/j.ijbiomac.2015.05.001

42. C. Fen, G. Sun, Z. Wang, X. Cheng, H. Park, D. Cha, M. Kong, X. Chen, Transport mechanism of doxorubicin loaded chitosan based nanogels across intestinal epithelium, Eur J Pharm Biopharm 87(1) (2014) 197–207. http://doi.org/10.1016/j.ejpb.2013.11.007

43. X. W, C. He, Y. Wu, X. Chen, J. Cheng, Nanogel-incorporated physical and chemical hybrid gels for highly effective chemo-protein combination therapy, Adv Funct Mater 25(43) (2015) 6744–6755. https://doi.org/10.1002/adfm.201502742

44. M. Rajan, V. Raj, A.A. Al-Arfaj, A.M. Murugan, Hyaluronidase enzyme core-5-fluorouracil-loaded chitosan-PEG-gelatin polymer nanocomposites as targeted and controlled drug delivery vehicles, Int J Pharm 453(2) (2013) 514–522. http://doi.org/10.1016/j.ijpharm.2013.06.030

45. G.I. Harisa, M.M. Badran, S.A. AlQahtan, F.K. Alanazi, S.M. Attia, Pravastatin chitosan nanogels-loaded erythrocytes as a new delivery strategy for targeting liver cancer, Saudi Pharm J 24(1) (2016) 74–81. http://doi.org/10.1016/j.jsps.2015.03.024

46. F. Sultana, M. Imran-Ul-Haque, M. Arafat, S. Sharmin, An overview of nanogel drug delivery system, J Appl Pharm Sci 3(8 SUPPL) (2013) 95–105. https://doi.org/10.7324/JAPS.2013.38.S15

47. S. Manivong, A. Garcia Ac, S.A. Patten, J.C. Fernandes, M. Benderdour, X. Banquy, F. Moldovan, V.G. Roullin, Chitosan-Based Nanogels: Synthesis and Toxicity Profile for Drug Delivery to Articular Joints, Nanomaterials 12(8) (2022) 1337–1354. https://doi.org/10.3390/nano12081337

48. W. Zou, D. Williams, A. Cox, Mitigating base-catalysed degradation of periodate-oxidized capsular polysaccharides: Conjugation by reductive amination in acidic media, Vaccine 37(8) (2019) 1087-1093. https://doi.org /10.1016/j.vaccine.2018.12.072

49. Z.W. Jing, Z.W. Ma, C. Li, Y. Y. Jia, M. Luo, X.X. Ma, S.Y Zhou, B.L. Zhang, Chitosan cross-linked with poly(ethylene glycol)dialdehyde via reductive amination as effective controlled release carriers for oral protein drug delivery, Bioorg Med Chem Lett 27(4) (2017) 1003-1006. https://doi.org/10.1016/j.bmcl.2016.12.072

50. S. Magli, G.B. Rossi, G. Risi, S. Bertini, C. Cosentino, L. Crippa, E. Ballarini, G. Cavaletti, L. Piazza, E. Masseroni, F. Nicotra, L. Russo, Design and synthesis of chitosan-gelatin hybrid hydrogels for 3D printable *in vitro* models, Front Chem 8 (524) (2020) 1-13. https://doi.org/10.3389/fchem.2020.00524

51 M. Montiel-Herrera, A. Gandini, F.M. Goycoolea, N.E. Jacobsen, J. Lizardi-Mendoza, M. Recillas-Mota, W.M. Argüelles-Monal, N-(furfural) chitosan hydrogels based on Diels-Alder cycloadditions and application as microspheres for controlled drug release, Carbohydr Polym 128 (2015) 220-227. https://doi.org/10.1016/j.carbpol.2015.03.052

52. L.M. Bravo-Anaya, K.G. Fernández-Solís, J. Rosselgong, J.L.E. Nano-Rodríguez, F. Carvajal, M. Rinaudo, Chitosan-DNA polyelectrolyte complex: Influence of chitosan characteristics and mechanism of complex formation, Int J Biol Macromol 126(126) (2019) 1037–1049. https://doi.org/10.1016/j.ijbiomac.2019.01.008

53. C.G. Gomez, M. Rinaudo, M.A. Villar Oxidation of sodium alginate and characterization of the oxidized derivatives, Carbohydr Polym 67(3) (2007) 296–304. https://doi.org/10.1016/j.carbpol.2006.05.025

54. R. Tripathi, S. Verma, J. Pandey, V. Tiwari, Recent development on catalytic reductive amination and applications, Curr Org Chem 12(13) (2008) 1093–1115. http://doi.org/10.2174/138527208785740283

55. H. Zhao, N.D. Heindel, Determination of degree of substitution of formyl groups in polyaldehyde dextran by the hydroxylamine hydrochloride method, Pharmaceutical Research: An Official Journal of the American Association of Pharmaceutical Scientists 8 (1991) 400–402. https://doi.org/10.1023/A:1015866104055

56. D. Paiva, C. Gonçalves, I. Vale, M.M.S.M. Bastos, F.D. Magalhães. Oxidized xanthan gum and chitosan as natural adhesives for cork, Polymers 8(7) (2016) 259–272. https://doi.org/10.3390/polym8070259

57. C. Schatz, S. Lougue, J-F. Le Meins, S. Lecommandoux, Polysaccharide- block - polypeptide Copolymer Vesicles: Towards Synthetic Viral Capsids, Angew Chemie 121(14) (2009) 2610–2613. http://doi.org/10.1002/anie.200805895

58. L.M. Bravo-Anaya, M. Rinaudo, F.A. Soltero Martínez, Conformation and rheological properties of calf-thymus DNA in solution, Polymers 8(51) (2016) 1–19. https://doi.org/10.3390/polym8020051

59. C.N. Costa, V.G. Teixeira, M.C. Delpech, J.V.S. Souza, M.A.S. Costa, Viscometric study of chitosan solutions in acetic acid/sodium acetate and acetic acid/sodium chloride, Carbohydr Polym 133 (2015) 245–250. http://doi.org/10.1016/j.carbpol.2015.06.094

60. V. Mirzaie, M. Ansari, S.N. Nematollahimahani, M.M. Nasery, B. Karimi, T. Eslaminejad, Y. Pourshojaei, Nano-graphene oxide-supported APTESspermine, as gene delivery system, for transfection of pEGFP-p53 into breast cancer cell lines, Drug Des Devel Ther 14 (2020) 3087–3097. https://doi.org/10.2147/DDDT.S251005

61. L. Xu L, F. Mallamace, Z. Yan Z, F.W. Starr, S.V. Buldyrev, H. Eugene Stanley, Appearance of a fractional stokes-einstein relation in water and a structural interpretation of its onset, Nat Phys 5(8) (2009) 565–569. https://doi.org/10.1038/nphys1328

62. S. Bhattacharjee, DLS and zeta potential - What they are and what they are not? J Control Release 235 (2016) 337–351. http://dx.doi.org/10.1016/j.jconrel.2016.06.017

63. F.L. Graham, J. Smiley, W.C. Russell, R. Nairn, Characteristics of a human cell line transformed by DNA from human adenovirus type 5, The Journal of General Virology. 36(1) (1977) 59–74. https://doi.org/10.1099/0022-1317-36-1-59

64. H. Dai, W. Yao, X. Zhou, Z. Tang, Q. Zhou, X. Li, Study of H_2O_2/Cu^{2+} catalyzed oxidation process of maltodextrin, Catalyst, 13(733) (2023) 1-9. https://doi.org/10.3390/catal13040733

65. S.D. Zhang, Y.R. Zhang, X.L. Wang, Y.Z. Wang, High carbonyl content oxidized starch prepared by hydrogen peroxide and its thermoplastic application, Starch/Staerke 61(11) (2009) 646–655. http://doi.org/10.1002/star.200900130

66. M. Rinaudo, Periodate oxidation of methylcellulose: Characterization and properties of oxidized derivatives, Polymers 2(4) (2010) 505–521. https://doi.org/10.3390/polym2040505

67. C.G. Gomez, M. Rinaudo, M.A. Villar, Oxidation of sodium alginate and characterization of the oxidized derivatives. Carbohydr Polym. 67(3) (2007) 296–304. https://doi.org/10.1016/j.carbpol.2006.05.025

68. K. Tømmeraas, K.M. Vårum, B.E. Christensen BE, O. Smidsrød, Preparation and characterisation of oligosaccharides produced by nitrous acid depolymerisation of chitosans, Carbohydr 333(2) (2001) 137–144. https://doi.org/10.1016/S0008-6215(01)00130-6

69. K. Parikka, M. Tenkanen, Oxidation of methyl α-d-galactopyranoside by galactose oxidase: products formed and optimization of reaction conditions for production of aldehyde, Carbohydr Res 344(1) (2009) 14–20. http://dx.doi.org/10.1016/j.carres.2008.08.020

70. N. Berriaud, M. Mila, M. Rinaudo M. Characterization and properties of hyaluronic acid (hyaluronan). In: D. Severian, editor, Polysaccharides in Medicine and Biotechnology 2nd ed. New York: Marcel Dekker, 2005, pp. 313–334. https://doi.org/10.1021/ja0410486

71. T.K. Kwei, M. Nakazawa, S. Matsuoka, M.K. Cowman, Y. Okamoto, Concentration dependence of solution viscosities of rigid rod polymers, Macromolecules 33(2) (2000) 235–236. https://doi.org/10.1021/ma9912002

72. E. Akiyama, N. Morimoto, P. Kujawa, Y. Ozawa, F.M. Winnik, K. Akiyoshi, Self-assembled nanogels of cholesteryl-modified polysaccharides: effect of the polysaccharide structure on their association characteristics in the dilute and semidilute regimes, Biomacromolecules 8(8) (2007) 2366–2373. https://doi.org/10.1021/bm070136q

73. S.A. Bencherif, D.J. Siegwart, A. Srinivasan, F. Horkay, J.O. Hollinger, N.R. Washburn K. Matyjaszewski, Nanostructured hybrid hydrogels prepared by a combination of atom transfer radical polymerization and free radical polymerization, Biomaterials 30(29) (2009) 5270–5278. http://dx.doi.org/10.1016/j.biomaterials.2009.06.011

74. R.J. Mayer, J. Moran, Quantifying reductive amination in nonenzymatic amino acid synthesis, Angew Chemie - Int Ed 61(48) (2022) e202212237 1-10. https://doi.org/10.1002/anie.202212237

75. S. Honary, F. Zahir, Effect of zeta potential on the properties of nano-drug delivery systems - A review (Part 1), Trop J Pharm Res 12(2) (2013) 255–64. https://doi.org/10.4314/tjpr.v12i2.20

76. S. Nimesh, M. M. Thibault, M. Lavertu, M. Michael D. Buschmann, Enhanced Gene Delivery Mediated by Low Molecular Weight Chitosan/DNA Complexes: Effect of pH and Serum, Mol Biotechnol 46 (2010) 182‑196. https://doi.org/10.1007/s12033-010-9286-1

77. H. Guo, F. Li, H. Qiu, Q. Zheng, C. Yang, C. Tang, Y. Hou, Chitosan-based nanogel enhances chemotherapeutic efficacy of 10-hydroxycamptothecin against human breast cancer cells, Int J Polym Sci 2019 (2019) 1–6. https://doi.org/10.1155/2019/1914976

78. H. Katas, H.O. Alpar, Development and characterisation of chitosan nanoparticles for siRNA delivery, J Control Release 115(2) (2006) 216–225. https://doi.org/10.1016/j.jconrel.2006.07.021

79. S. Hassanpour, F. Farshi Azhar, M. Bagheri, Novel nanogels based on hydroxypropyl cellulose–poly(itaconic acid) for adsorption of methylene blue from aqueous solution: process modeling and optimization using response surface methodology, Polym Bull 76(2) (2019) 933–952. https://doi.org/10.1007/s00289-018-2419-6

80. Y. Zhao, C. Simon, M. Daoud Attieh, K. Haupt, A. Falcimaigne-Cordin, Reduction-responsive molecularly imprinted nanogels for drug delivery applications, RSC Adv 10(10) (2020) 5978–5987. https://doi.org/10.1039/C9RA07512G

81. F. Damiri, A. Fatimi, A.C.P. Santos, R.S. Varma, M. Berrada, Smart stimuli-responsive polysaccharide nanohydrogels for drug delivery: a review, J Mater Chem B 11 (2023) 10538-10565. https://doi.org/10.1039/D3TB01712E

82. N. Sanson, J. Rieger Synthesis of nanogels/microgels by conventional and controlled radical crosslinking copolymerization, Polym Chem 1(7) (2010) 965–977. https://doi.org/10.1039/C0PY00010H

83. S. Tang, Z. Shi, Y. Cao, W. He, Facile aqueous-phase synthesis of multi-responsive nanogels based on polyetheramines and bisepoxide, J Mater Chem B 1(11) (2013) 1628–1634. https://doi.org/10.1039/C3TB00492A

Captions

Scheme 1. a) MD oxidation with sodium periodate [53]; b) reductive amination between oxidized MD and CS in the presence of sodium cyanoborohydride [54]; c) schematic representation of MD/CS nanogels. Yellow links in the nanogel correspond to the resulting covalent bond from reductive amination.

Scheme 2. Reductive amination between oxidized MDs and butylamine in the presence of sodium cyanoborohydride.

Fig. 1.- FTIR spectra for the initial MD and the ox-MD samples with different degrees of oxidation.

Fig. 2.- ^{1}H NMR spectra in D_2O at 25 °C for: a) MD, and ox-MD samples with targeted oxidation degrees of b) 10 % and c) 30 %.

Fig. 3.- Size distribution, obtained from DLS measurements, for MD/CS nanogels synthesized by using HMW CS at a pH of 5.5, 11 % ox-MD and at CS concentrations equivalent to C*/5, C*/2, C*, 2C*, 3C* and 5C*.

Fig. 4.- a) Effect of CS DA on MD/CS nanogels hydrodynamic diameter. CS #6 (DA=0.05) and CS #8 (DA=0.47) were selected as examples. b) Effect of pH (3.5 and 5.5) on MD/CS nanogels hydrodynamic diameter (48 % ox-MD). Three CS samples were selected as examples (CS #1, CS #6 and CS #8). c) Effect of ox-MD (11 and 48 % ox-MD) on MD/CS nanogels hydrodynamic diameter. Three CS samples were selected as examples (CS #1, CS #6 and CS #8).

Fig. 5.- a) SEM image, b) zoom-in and c) size distribution obtained for MD/CS nanogels. MD/CS nanogels were synthesized using CS #1 (C_{CS} = 1 mg/mL, DA = 0.30, pH = 5.5) and 48 % ox-MD.

Fig. 6.- a) Intensity distribution as a function of D_H for MD/CS nanogels measured each week. b) Evolution of D_H and PDI as a function of time in weeks. c) Evolution of D_H and ζ-potential as a function of pH. MD/CS nanogels were prepared with CS HMW (C_{CS} = 1.2 mg/mL, DA = 0.16, pH = 5.5) and 48 % ox-MD.

Fig. 7.- Cell viability assays (relative ATP content) were performed after 48 hours of HEK exposure to nanogels. MD/CS nanogel 1 was prepared with CS #6 (C_{CS} = 0.1 mg/mL, DA =

0.05, pH = 5.5) and 48 % ox-MD; MD/CS nanogel 2 was prepared with CS #1 (C_{CS} = 0.03 mg/mL, DA = 0.05, pH = 5.5) and 48 % ox-MD.

Tables

Table 1. Degree of oxidation for MD samples as determined by titration with $NH_2 \cdot HCl$.

Table 2. Degree of protonation of CS samples at a pH of 5.5 determined through potentiometric titration of CS solutions.

Table 3.- Intrinsic viscosity [η] and overlap concentration (C*) for all CS samples, determined through viscosity measurements.

Table 4.- Hydrodynamic diameter (D_H) for some representative MD/CS nanogels synthesized using the three CS samples at different CS concentrations, two pH values (3.5 and 5.5) and two MD oxidation degrees.

Table 5.- ζ-potential for some representative MD/CS nanogels synthesized using the three CS samples at different CS concentrations, two pH values (3.5 and 5.5) and two MD oxidation degrees.

Scheme 1.

International Journal of Biological Macromolecules

Karla Gricelda Fernández-Solís, Estefanía Domínguez-Fonseca, Brianda María González Martínez, Alberto Gutiérrez Becerra, Edgar Figueroa Ochoa, Eduardo Mendizábal, Guillermo Toriz, Pascal Loyer, Julien Rosselgong, Lourdes Mónica Bravo-Anaya

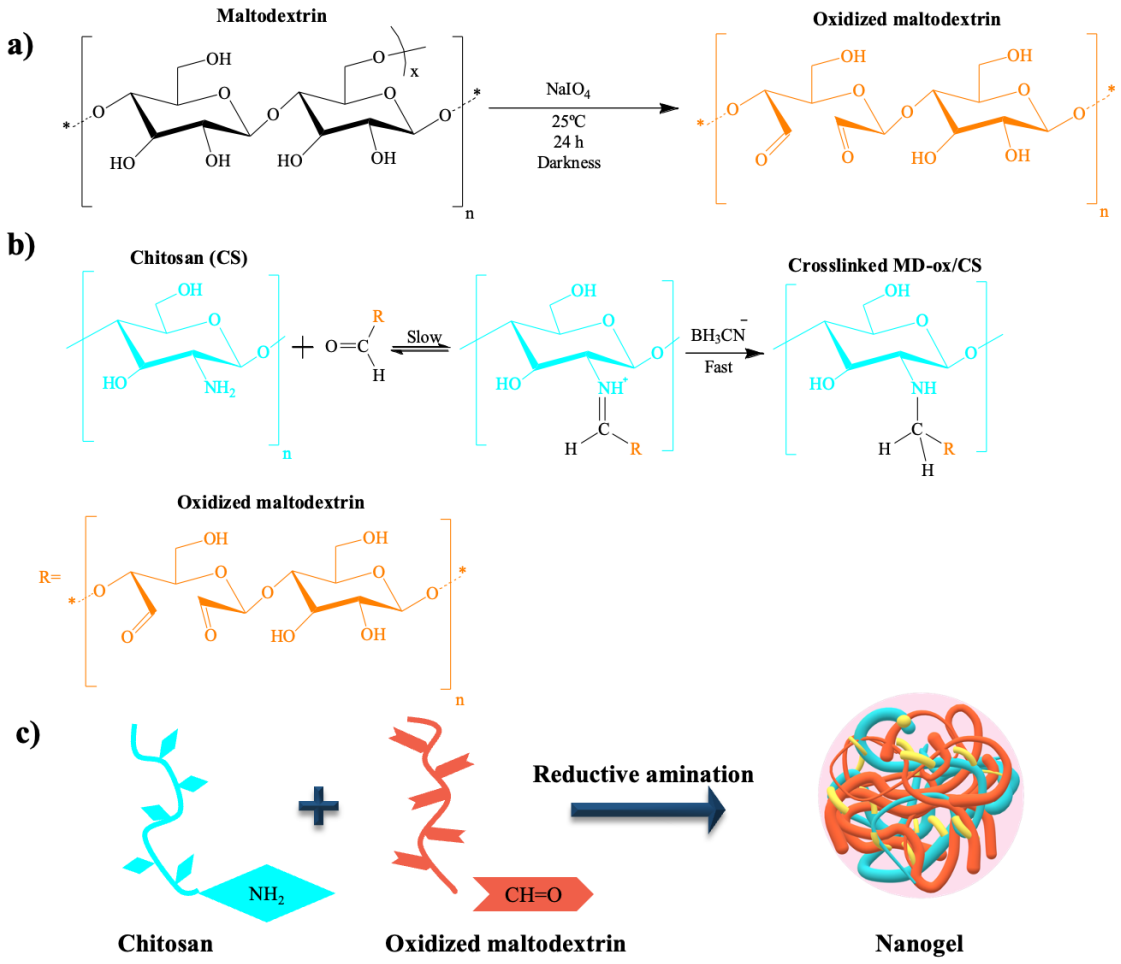

Scheme 2.

International Journal of Biological Macromolecules

Karla Gricelda Fernández-Solís, Estefanía Domínguez-Fonseca, Brianda María González Martínez, Alberto Gutiérrez Becerra, Edgar Figueroa Ochoa, Eduardo Mendizábal, Guillermo Toriz, Pascal Loyer, Julien Rosselgong, Lourdes Mónica Bravo-Anaya

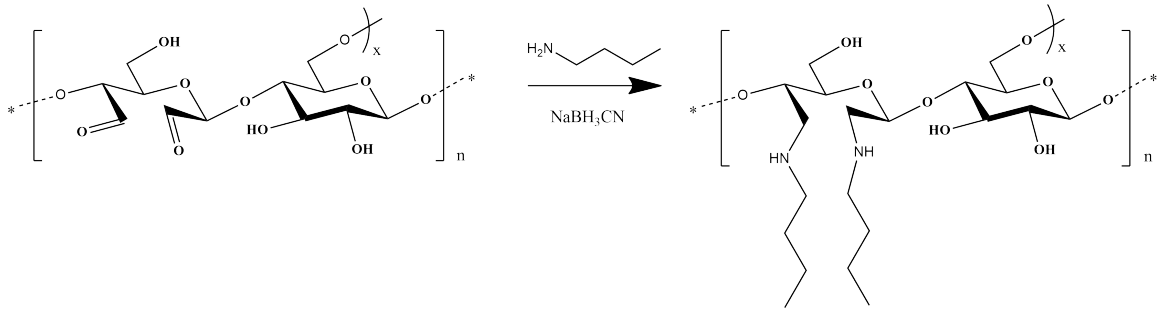

Fig. 1.

International Journal of Biological Macromolecules

Karla Gricelda Fernández-Solís, Estefanía Domínguez-Fonseca, Brianda María González Martínez, Alberto Gutiérrez Becerra, Edgar Figueroa Ochoa, Eduardo Mendizábal, Guillermo Toriz, Pascal Loyer, Julien Rosselgong, Lourdes Mónica Bravo-Anaya

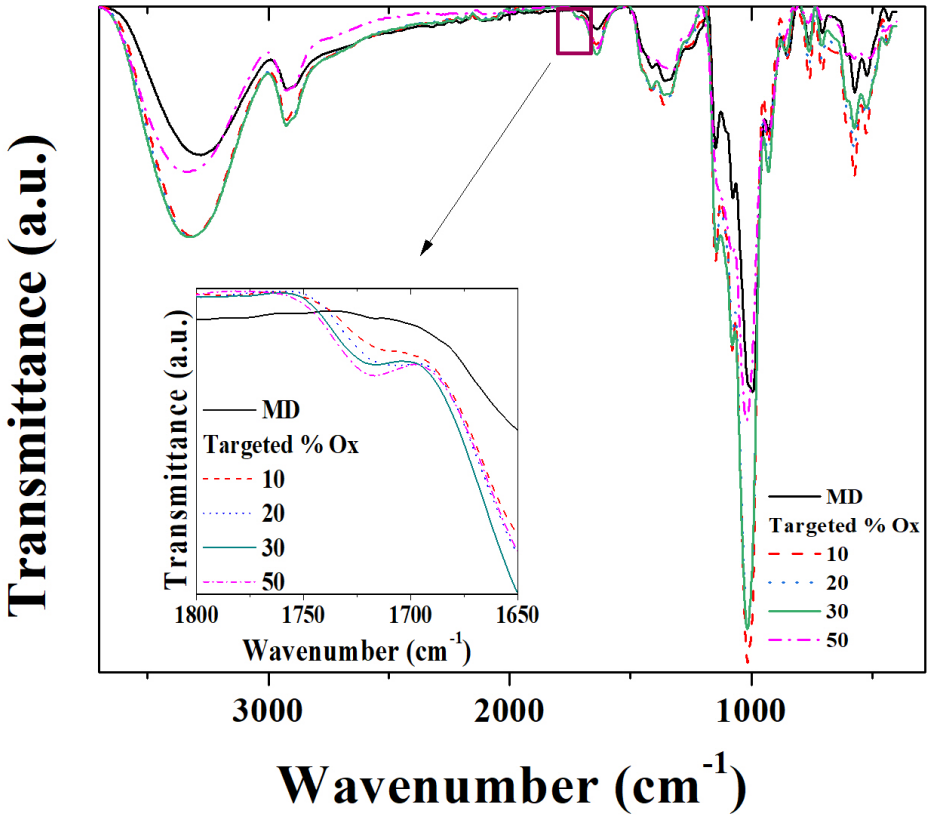

Fig. 2.

International Journal of Biological Macromolecules

Karla Gricelda Fernández-Solís, Estefanía Domínguez-Fonseca, Brianda María González Martínez, Alberto Gutiérrez Becerra, Edgar Figueroa Ochoa, Eduardo Mendizábal, Guillermo Toriz, Pascal Loyer, Julien Rosselgong, Lourdes Mónica Bravo-Anaya

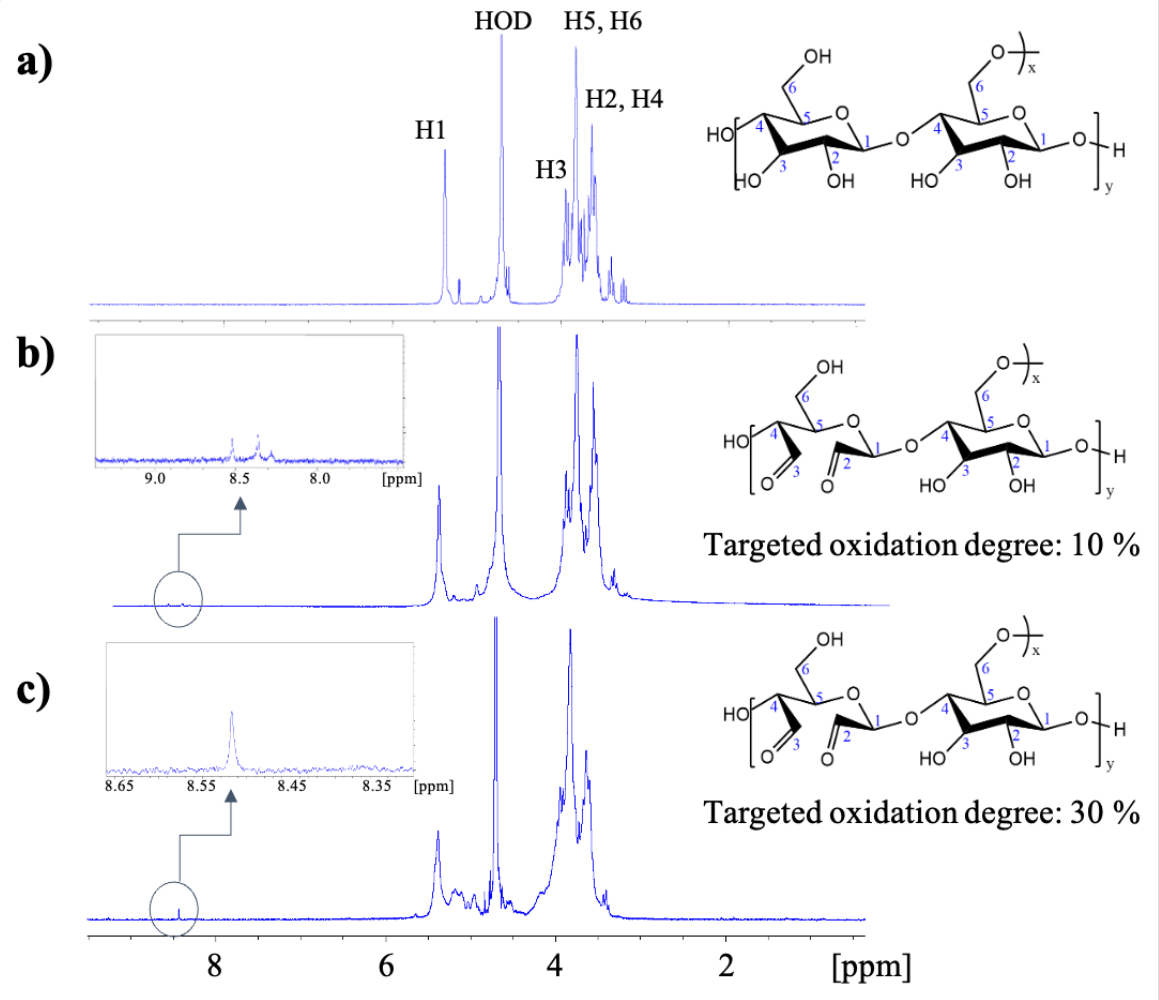

Fig. 3.

International Journal of Biological Macromolecules

Karla Gricelda Fernández-Solís, Estefanía Domínguez-Fonseca, Brianda María González Martínez, Alberto Gutiérrez Becerra, Edgar Figueroa Ochoa, Eduardo Mendizábal, Guillermo Toriz, Pascal Loyer, Julien Rosselgong, Lourdes Mónica Bravo-Anaya

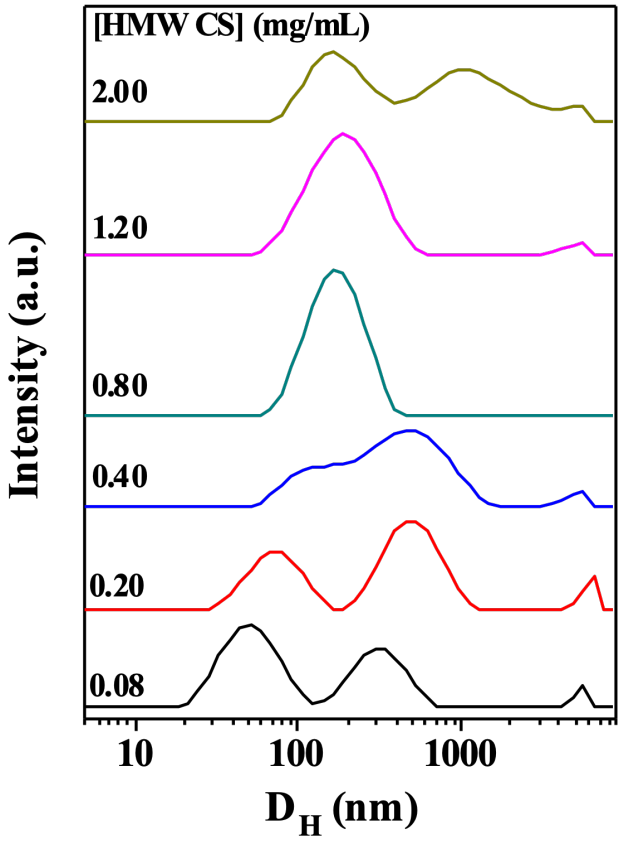

Fig. 4.

International Journal of Biological Macromolecules

Karla Gricelda Fernández-Solís, Estefanía Domínguez-Fonseca, Brianda María González Martínez, Alberto Gutiérrez Becerra, Edgar Figueroa Ochoa, Eduardo Mendizábal, Guillermo Toriz, Pascal Loyer, Julien Rosselgong, Lourdes Mónica Bravo-Anaya

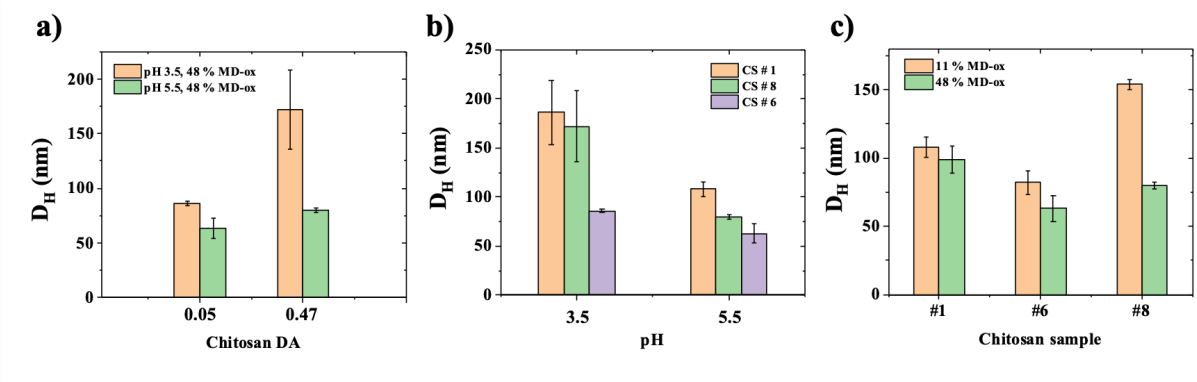

Fig. 5.

International Journal of Biological Macromolecules

Karla Gricelda Fernández-Solís, Estefanía Domínguez-Fonseca, Brianda María González Martínez, Alberto Gutiérrez Becerra, Edgar Figueroa Ochoa, Eduardo Mendizábal, Guillermo Toriz, Pascal Loyer, Julien Rosselgong, Lourdes Mónica Bravo-Anaya

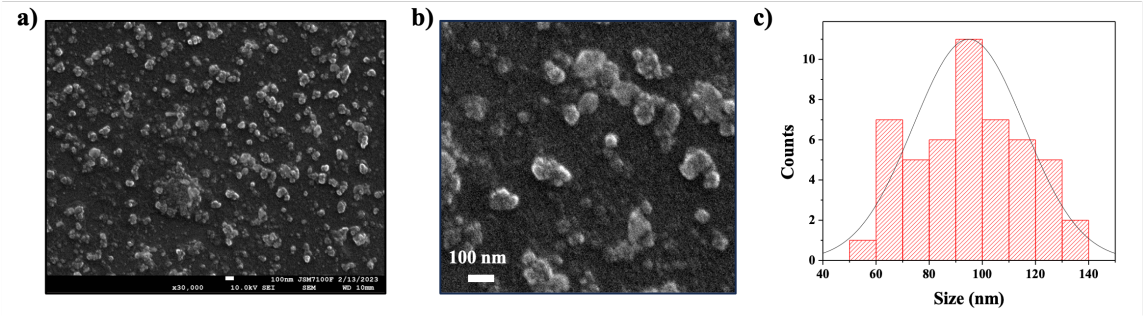

Fig. 6.

International Journal of Biological Macromolecules

Karla Gricelda Fernández-Solís, Estefanía Domínguez-Fonseca, Brianda María González Martínez, Alberto Gutiérrez Becerra, Edgar Figueroa Ochoa, Eduardo Mendizábal, Guillermo Toriz, Pascal Loyer, Julien Rosselgong, Lourdes Mónica Bravo-Anaya

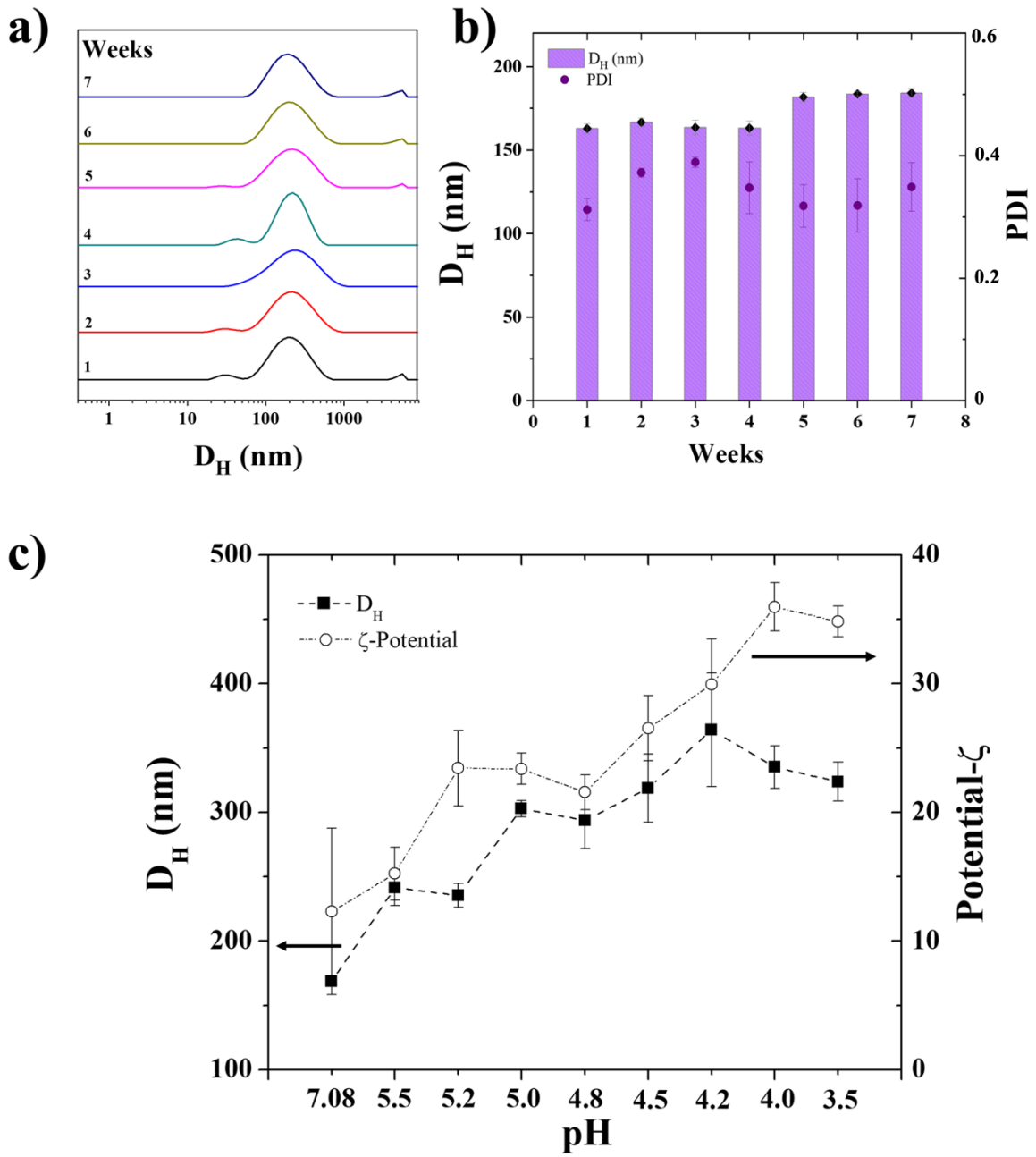

Fig. 7.

International Journal of Biological Macromolecules

Karla Gricelda Fernández-Solís, Estefanía Domínguez-Fonseca, Brianda María González Martínez, Alberto Gutiérrez Becerra, Edgar Figueroa Ochoa, Eduardo Mendizábal, Guillermo Toriz, Pascal Loyer, Julien Rosselgong, Lourdes Mónica Bravo-Anaya

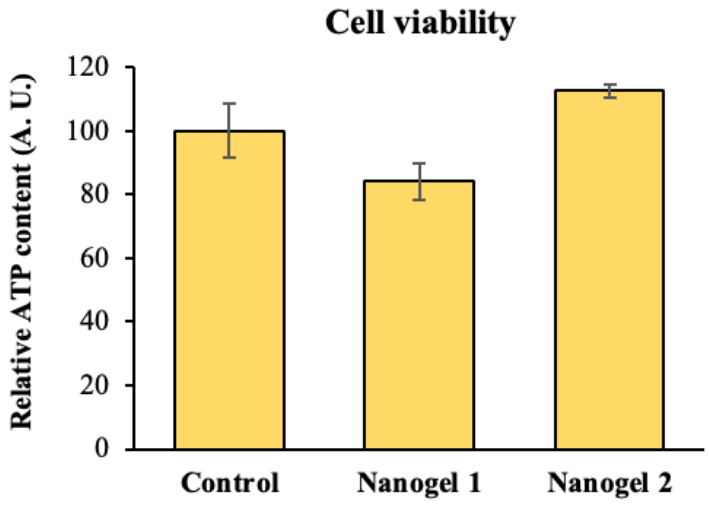

Table 1.

International Journal of Biological Macromolecules

Karla Gricelda Fernández-Solís, Estefanía Domínguez-Fonseca, Brianda María González Martínez, Alberto Gutiérrez Becerra, Edgar Figueroa Ochoa, Eduardo Mendizábal, Guillermo Toriz, Pascal Loyer, Julien Rosselgong, Lourdes Mónica Bravo-Anaya

Maltodextrin sample	Targeted oxidation degree (%)	Real oxidation degree (%)
Ox-MD-1	10	11
Ox-MD-2	20	24
Ox-MD-3	30	48
Ox-MD-4	50	58

Table 2.

International Journal of Biological Macromolecules

Karla Gricelda Fernández-Solís, Estefanía Domínguez-Fonseca, Brianda María González Martínez, Alberto Gutiérrez Becerra, Edgar Figueroa Ochoa, Eduardo Mendizábal, Guillermo Toriz, Pascal Loyer, Julien Rosselgong, Lourdes Mónica Bravo-Anaya

Chitosan sample	Protonation degree at pH = 5.5 (%)
#1	73.5
#6	53.5
#8	41.2
MMW	63.0
HMW	53.5

Table 3.

International Journal of Biological Macromolecules

Karla Gricelda Fernández-Solís, Estefanía Domínguez-Fonseca, Brianda María González Martínez, Alberto Gutiérrez Becerra, Edgar Figueroa Ochoa, Eduardo Mendizábal, Guillermo Toriz, Pascal Loyer, Julien Rosselgong, Lourdes Mónica Bravo-Anaya

Chitosan sample	[η] (mL/g)	C* (mg/mL)
# 1	3 333	0.3
# 6	1 000	1.0
# 8	714	1.4
MMW	700	1.4
HMW	2 500	0.4

Table 4.

International Journal of Biological Macromolecules

Karla Gricelda Fernández-Solís, Estefanía Domínguez-Fonseca, Brianda María González Martínez, Alberto Gutiérrez Becerra, Edgar Figueroa Ochoa, Eduardo Mendizábal, Guillermo Toriz, Pascal Loyer, Julien Rosselgong, Lourdes Mónica Bravo-Anaya

Chitosan	DA	[CS] (mg/mL)	pH	ox-MD (%)	D_H (nm)	PDI
# 1	0.30	0.03	3.5	11	186 ± 32	0.370 ± 0.066
# 1	0.30	0.03	5.5	11	108 ± 7	0.275 ± 0.077
# 1	0.30	0.03	3.5	48	89 ± 7	0.266 ± 0.032
# 1	0.30	0.03	5.5	48	99 ± 10	0.179 ± 0.073
# 6	0.05	0.10	3.5	11	419 ± 93	0.137 ± 0.076
# 6	0.05	0.10	5.5	11	82 ± 8	0.279 ± 0.069
# 6	0.05	0.10	3.5	48	86 ± 2	0.217 ± 0.003
# 6	0.05	0.10	5.5	48	63 ± 9	0.155 ± 0.053
# 8	0.47	0.14	3.5	11	279 ± 16	0.362 ± 0.010
# 8	0.47	0.14	5.5	11	154 ± 4	0.339 ± 0.002
# 8	0.47	0.14	3.5	48	172 ± 36	0.216 ± 0.168
# 8	0.47	0.14	5.5	48	80 ± 2	0.259 ± 0.033

Table 5.

International Journal of Biological Macromolecules

Karla Gricelda Fernández-Solís, Estefanía Domínguez-Fonseca, Brianda María González Martínez, Alberto Gutiérrez Becerra, Edgar Figueroa Ochoa, Eduardo Mendizábal, Guillermo Toriz, Pascal Loyer, Julien Rosselgong, Lourdes Mónica Bravo-Anaya

Chitosan	DA	[CS] (mg/mL)	pH	ox-MD (%)	ζ-potential (mV)
# 1	0.30	0.015	3.5	11	+ 14 ± 1.6
# 1	0.30	0.015	5.5	11	+ 4 ± 0.2
# 1	0.30	0.03	3.5	48	+ 30 ± 1.5
# 1	0.30	0.03	5.5	48	+ 16 ± 2.6
# 6	0.05	0.10	3.5	11	+ 36 ± 2.0
# 6	0.05	0.10	5.5	11	+ 24 ± 2.8
# 6	0.05	0.10	3.5	48	+ 24 ± 0.9
# 6	0.05	0.10	5.5	48	+ 9 ± 1.4
# 6	0.05	0.05	5.5	48	+ 3 ± 0.2
# 6	0.05	1.00	5.5	48	+ 34 ± 1.0
# 8	0.47	0.07	5.5	48	+ 4 ± 0.2
# 8	0.47	1.40	5.5	48	+22 ± 0.3